



# Fractal discrete fracture network modeling of radon gas concentration in underground tunnels under Książ Castle in Poland

Lidia Fijałkowska–Lichwa<sup>1</sup> · Kayode M. Ajayi<sup>2</sup>

Received: 15 January 2024 / Accepted: 22 May 2024  
© The Author(s) 2024

## Abstract

The numerical modeling of radon concentrations in the fault zone of the underground excavations at Książ Castle was conducted using a stochastic Discrete Fracture Network (DFN) model. Due to the difficulties related with obtaining the exact fractures in a rock mass, the novel approach used in this study incorporates the stochastic model with known site data. The analysis utilized a dataset comprising long-term measurements of  $^{222}\text{Rn}$  activity concentration and geodetic measurements for twelve faults in the Książ unit. The parameters considered in the DFN model are: fracture length, Peclet number ( $Pe = 0.1$  and  $1.0$ , respectively), advection velocities (from  $10^{-8}$  m/s to  $10^{-6}$  m/s and from range from  $10^{-7}$  m/s to  $10^{-4}$  m/s, respectively), radon diffusion ( $D = 2.1 \times 10^{-6}$  m<sup>2</sup>/s), radon decay constant ( $\lambda = 1/\text{s}$ ), and radon gas generation ( $q$ ) along the fractures within the range of  $1.5 \times 10^{-3}$  Bq/m<sup>3</sup>·s to  $3.5 \times 10^{-3}$  Bq/m<sup>3</sup>·s. The calibration process obtained the best fit when the radon generation rate was uniformly distributed through the rock mass in addition to incorporating a higher value of radon generation rate ( $q = 3.0 \times 10^{-3}$  Bq/m<sup>3</sup>·s) where elevated radon concentrations have been measured. The modeling results also confirmed that the radon generation rate should always be higher where elevated radon activity concentrations were measured regardless of the measurement period. For the indicated “area” the radon generation rate should be higher from 25% to 37.5% between May–October and 18.5% to 40% between November–April. The influence of fracture zones on the recorded radon activity concentrations was noticeable up to a depth of 15 m. Within this range, the highest values of  $^{222}\text{Rn}$  activity concentration, ranging from 1,600 Bq/m<sup>3</sup> to 2,000 Bq/m<sup>3</sup>, were consistently observed regardless of the season. However, as the depth increased, the values of  $^{222}\text{Rn}$  activity concentration decreased from 800 Bq/m<sup>3</sup> to 400 Bq/m<sup>3</sup> and became more dispersed.

**Keywords** Discrete fractal network (DFN) model; radon gas · Faults ·  $^{222}\text{Rn}$  activity concentration measurements · Underground tunnels · Stochastic methods

## Introduction

The latest research advancements on radon involve utilizing radon time series data to measure the radon flow (Alhmadi and Abdullah, 2021; Girault et al. 2022; Haquin et al. 2021;

MiklyaeV and Petrova 2021; Muhammad and Kùlahcı 2022; Rafique et al. 2022; Chen et al. 2023; Lei et al. 2023; Wang et al. 2024). With underground systems, the prediction of radon’s behaviour depends strongly on the identification of patterns hidden in the associated time series. Hence, numerous studies employ a closed-system model, reinforced by statistical and numerical analyses, to comprehend the mechanisms governing radon transportation and variations in concentration. These analyses predominantly include methods such as Empirical Mode Decomposition-based Hilbert–Huang transform, Multiple Linear Regression, Artificial Neural Network techniques, Monte Carlo simulations, chaos theory, decomposition methods, machine learning, standard deviation analysis, and stacking methods.

Based on these fundamentals, it becomes feasible to ascertain the vertical movement of radon and its flow parameters across daily, seasonal, and yearly timescales. Li et al.

### Highlights

- A DFN model was developed to predict radon gas concentrations at the dislocation zone (12 faults) described by geodetic methods in an underground excavation in Poland.
- Long-term  $^{222}\text{Rn}$  activity concentration measurements were used to validate the stochastic DFN model.
- Radon generation rate in the immediate vicinity of the fault was calibrated to reflect results obtained from field measurements.
- Regardless of the season of measurements, a 40% higher radon generation rate is proposed for the regions where notably elevated radon activity concentrations have been measured.

Extended author information available on the last page of the article

(2024) conducted research in the Mogao Grottoes (north-west China), concluding that variations in earth-air flow and radon concentration are contingent upon atmospheric pressure fluctuations. A decrease in atmospheric pressure leads to earth-air outflows from soil with high radon concentration, while the reverse occurs when the atmospheric pressure rises. Nevertheless, surface closure, landform, cracks, faults, grain size, pore structure, soil adsorption, basal uranium/radium content, salts, wind, lunar cycle, latitude, and altitude exert significant influences on radon exhalation rates. Studies by Li et al. (2024) corroborated that the amount of radon exhalation correlates with the amplitude of external atmospheric pressure fluctuations, the thickness of the investigated zone, and soil porosity. The higher radon values are emitted in summer and lower in winter, and vary seasonally with temperature and atmospheric pressure.

Sajwan et al. (2024) noted that fluctuations in radon data are linked to the enhanced permeability of fracture systems, which in turn influences the gas-bearing capacity of faults. Nonetheless, the uneven permeability of fractures results in the patchy distribution of soil-gas anomalies. Comparable findings were also reported by Prasetyo et al. (2023). They confirmed that geogenic gas, as radon ( $^{222}\text{Rn}$ ) can be widely used to infer permeability zones in some geological settings such as fault zones: Pejaten Fault, Banjarsari Fault and Cibitung Fault, volcanic and geothermal areas: Wayang Windu geothermal area. Li et al. (2022) also presented similar results for the mining area of northern Shaanxi, China. They confirmed a significant positive correlation between the radon exhalation rate and the microporosity. Among all investigated lithologies, the soil had the largest radon exhalation rate due a large amount of storage space and transport channels. Research made by Sajwan et al. (2024) noticed that mass exhalation rates and uranium concentration are significantly influenced in tectonically active areas.

Furthermore, research conducted by Thuamthansanga and Tiwari (2022) corroborated that the rates of soil radon production and exhalation are contingent on depth and exhibit distinct correlations with geophysical phenomena along the Indo-Burman subduction region. A strong correlation coefficient was visible during the non-anomaly period between the radon activity and exhalation rate while a weak or insignificant correlation coefficient during the anomaly period. Miklayev et al. (2022) suggested that radon release is caused by a single mechanism (convective), probably connected with the atmospheric air circulation in shallow permeable zones due to the temperature difference between the inside mountain and ambient atmosphere (called “breathing mountain”).

Over the past few years, radon ( $^{222}\text{Rn}$ ) activity concentration measurements have been conducted at a large underground space in Poland. The measurements are near the faults zone recognized in the corridors of the

underground complex under one of the largest castles in Poland (Fijałkowska-Lichwa and Przylibski 2016, 2021; Fijałkowska-Lichwa 2020). These measurements provide an insight into potential variation in the gas concentrations during any period (season, day, or transitional period). Given the results, seasonal changes observed in the annual cycle are typical for many underground facilities in the world (Barbosa et al. 2010; vási et al. 2010; Vaupotič et al. 2010; Alvarez-Gallego et al. 2015; Gillmore et al. 2005; Groves-Kirby et al. 2015; Tchorz-Trzeciakiewicz and Parkitny 2015; Kleinschmidt et al. 2018; Smith et al. 2019; Pla et al. 2020, 2023; Ambrosino et al. 2020; Smetanová et al. 2023; Miklayev et al. 2024). Daily changes in  $^{222}\text{Rn}$  activity concentrations are not significant but are dependent on the seasonal changes. The identified concentrations differed by no more than 10% from the corresponding mean values. The short-term changes recognized in transitional periods occurred from April to October when air movement was very slow, obstructed, or completely stopped (Fijałkowska-Lichwa and Przylibski 2011, 2016, 2021, 2023; Fijałkowska-Lichwa 2020). The findings show that radon propagation has a spatial character, not limited only through fault zones. The changes in  $^{222}\text{Rn}$  activity concentrations are visible in the excavations surrounding the fractured rocks and in non-fractured rock mass that are well insulated. The patterns of these changes are almost identical, and the difference between the absolute values of  $^{222}\text{Rn}$  activity concentrations recorded in these periods is significant.

Based on these findings, the researchers used radon as a tracer to recognize the mechanism of radon flux from the faults in non-isolated rocks surrounding the workings. To estimate the radon generation (exhalation) rate, long-term radon activity measurements conducted inside the object directly in the fault zone as well as in the entire corridor system (mainly non-tourist) are used. The findings from these measurements provide insights into the pattern and trends of radon concentration throughout the year. However, there are limitations (represented by specific radon migration pathways like: porous media or crashed rocks in dislocation zones) to the application of these measurements for investigating radon flux and the impact of different parameters on radon transport. Therefore, the objective of this study is also to develop a numerical model that could replicate the radon measurements.

The numerical modeling approach can be classified into discrete or continuum methods. In the continuum approach, transport properties are presumed to be uniformly distributed throughout the rock mass. However, this assumption does not accurately reflect field conditions, as fractures serve as the primary conduits for fluid flow. Therefore, the discrete approach is preferred, as it explicitly models fractures and assumes that their permeability is orders of magnitude greater than that of the rock matrix. Nonetheless, a limitation

of this approach is the inability to collect all fracture parameters for a rock mass during field studies. Hence, this study employs a novel approach that integrates a stochastic model with known site data. The model is calibrated based on the site condition with the assumption that most of the observed radon activity concentrations are from faults and fractures. It is intended that this model could be used for further predictive modeling under different conditions after it is validated with the field measurements.

## 2. Research approach

### 2.1. Description of the site, rock characteristics, and faults

The study site is located within the Riese complex, constructed by the German paramilitary organization Todt in the Sowie Mountains during World War II, specifically in the years 1943–1945 (Pawlikowska 2008). The site comprises a system of underground tunnels beneath the cour d'honneur of Książ Castle, divided into two parts: the non-tourist section and the tourist route. The Geodynamic Laboratory (GL) of the Space Research Centre of the Polish Academy of Sciences (SRC PAS) is situated in the non-tourist section, which was established in the mid-1970s (Kaczorowski 1999; Kaczorowski et al. 2012). This laboratory facilitates research on non-tidal processes, including kinematic effects in the rock massif (Kaczorowski and Wojewoda 2011; Kasza 2014). The tourist route, accessible to visitors since October 15, 2018, is the second part of the site (Fijałkowska-Lichwa and Przylibski 2021).

The study site is situated within the Książ massif, specifically the Książ morphological elevation, which represents the central part of the Świebodzice Unit (Fig. 1b). The area is characterized by an intricate network of faults (Fig. 1a, c). The Świebodzice Unit is bounded by several dislocation zones: the Sudetic marginal fault separates it from the fore-Sudetic block to the northeast, the Szczawienko fault acts as a boundary along with the Owl Mountain gneiss block to the south, and the Cieszów metamorphic complex marks the northern border. These dislocation zones define the borders with adjacent units such as the Pogorzała Formation, Pełcznica Formation, Książ Formation, and Chwaliszów Formation (Fig. 1b, Żelaźniewicz and Aleksandrowski, 2008). The formations mainly consist of carboniferous sedimentary rocks (Porębski 1981). Within the Świebodzice Unit, the sedimentary rocks exhibit strong local folding, with mesofolds primarily oriented in the west-east direction. The faults in the study site are well-recognized within the highly deformed Książ Formation (Fig. 1a, c). The Książ Formation comprises coarse-grained, poorly sorted conglomerates containing individual clasts (grains) reaching a maximum

diameter of 2 m. The framework grains consist of gneisses, migmatites, and granites, with sub-angular limestone clasts mixed in. The Książ Formation within the Książ massif displays significant deformation (Fig. 1a), and the faults indicate recent activity (Kasza et al. 2018).

### 2.2. Radon concentration measurement at the site

The data for this study was obtained from continuous  $^{222}\text{Rn}$  activity measurements conducted between June 2014 and October 2020. Five semiconductor SRDN-3 detectors (probes no. 2–6) were used, operating in 1-hour mode throughout the entire observation period on an annual basis. The using semiconductor detectors SRDN-3 were designed and built at the Institute of Chemistry and Nuclear Technology in Warsaw (Przylibski et al. 2010). The probes have been adapted to operate in a high-humidity and low-temperature environment like underground facilities, corridors, mining plants. The detectors are used for passive registration of radon activity concentrations using the diffusion phenomenon. Radon flows through the air inlet, protected by an air filter from contamination with dust particles, into the semiconductor detector chamber. In the detection chamber, radon nuclei decay and emits  $\alpha$  particles. This initiates the flow of electric current which is then measured and registered in the probe microcomputer. The  $\alpha$ -emission is counted as a pulse during a given time interval in the microcomputer counter. The automatic recording of the number of counts is repeated until the data memory is full. Then the data are removed or a new measurement cycle is started (Przylibski et al. 2010). Before the first in-situ measurements, the probes were calibrated for 24 successive hours in the conditions of known  $^{222}\text{Rn}$  activity concentration (484, 990, 4740 and 8873  $\text{Bq/m}^3$ ) pre-set in the radon chamber of the Institute of Nuclear Physics, Polish Academy of Sciences in Kraków. The conditions were controlled with a reference device AlphaGUARD. The number of pulses counted by the semiconductor detectors of SRDN-3 radon probes was compared with the values of  $^{222}\text{Rn}$  activity concentration recorded by the AlphaGUARD device. On this basis, the lower limits of detection (LLD) equalling 96.5  $\text{Bq/m}^3$ , 94.8  $\text{Bq/m}^3$ , 94.0  $\text{Bq/m}^3$ , 96.3  $\text{Bq/m}^3$  and 95.0  $\text{Bq/m}^3$  were determined for the detectors of radon probes No. 2, 3, 4, 5 and 6 respectively (Przylibski et al. 2010).

The radon activity concentrations were most observed within five ranges of values (Fig. 2a). Approximately 60% of the data recorded by probe no. 6 fell within the range of 500  $\text{Bq/m}^3$  and around 50% for probe no. 5 (Fig. 2a). Values of 1000  $\text{Bq/m}^3$  were reported by probes no. 5 and 6 (over 30%), as well as probe no. 3 (over 45%). Radon activity concentrations within the range of 1500  $\text{Bq/m}^3$  were measured by probes no. 2 and 3 (over 20%). The highest values, within the range of 2,500  $\text{Bq/m}^3$  and 3,000  $\text{Bq/m}^3$ , were exclusively

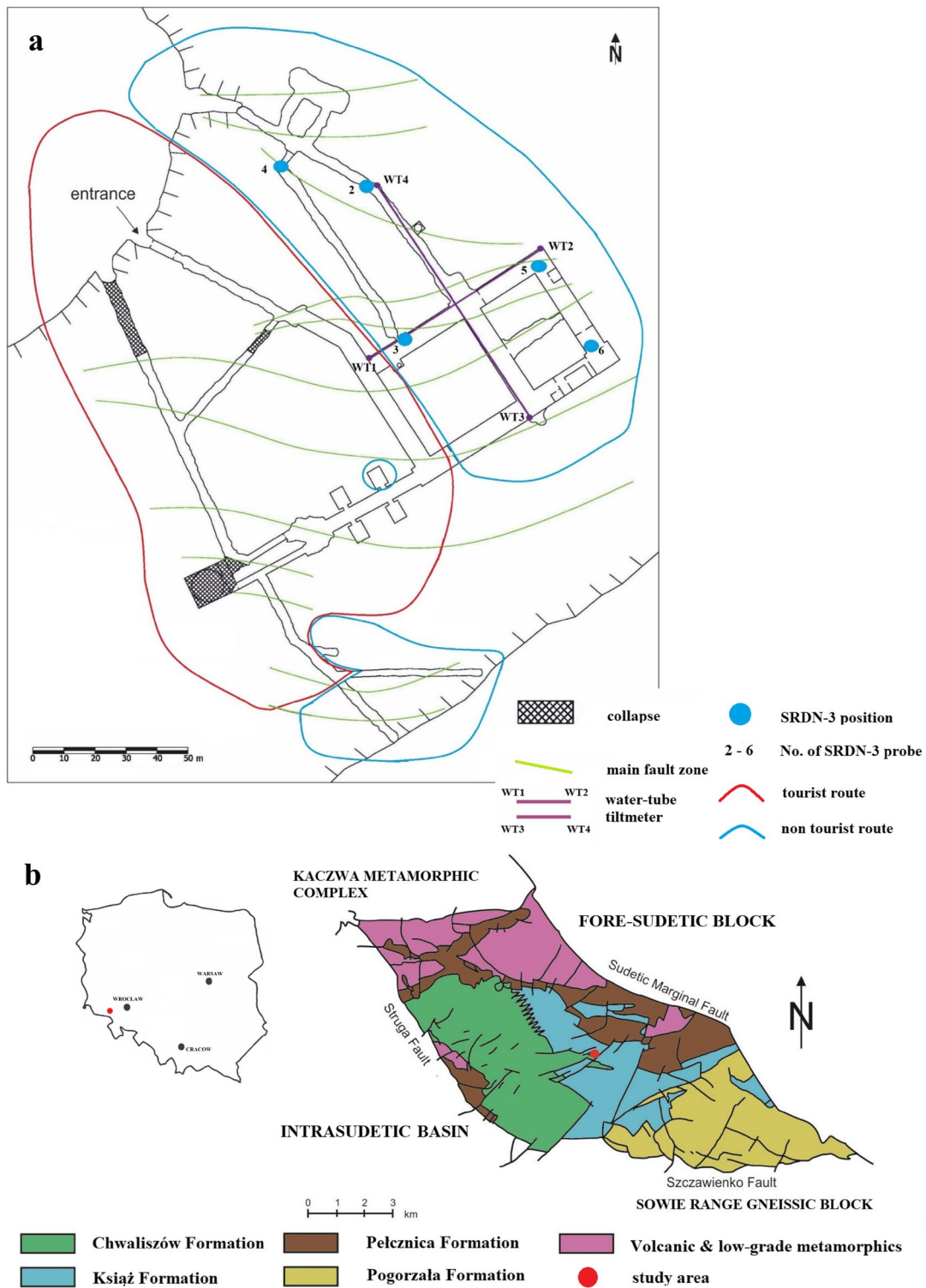


**Fig. 1** Location of 12 main faults recognized by Kasza and co-authors (2014, 2018) in study area on a simplified geological map of the Sudetes (b) and the radon measuring positions on a plan of the underground tourist and non-tourist tunnels under Książ Castle (a) (based on Kaczorowski and Wojewoda 2011 ; and Kasza et al. 2018 ; Przylibski et al. 2020 ). Cross-sections (c): A-A' – NW direction through WT1-2; B-B' - NW direction through WT3-4. Colors represent tectonic block divided by the recognized tectonic faults (based

on Przylibski et al. 2020 ).

Explanations: blue points represent SRDN-3 positions, the numbers 2–6 represent no. of SRDN-3 probe, red line represents tourist part of undergrounds, blue line represents non-tourist part, used by the Geodynamic Laboratory (GL) of the Space Research Centre of the Polish Academy of Sciences (SRC PAS), purple lines represent the location of water tube tiltmeters, green lines represent man fault zones

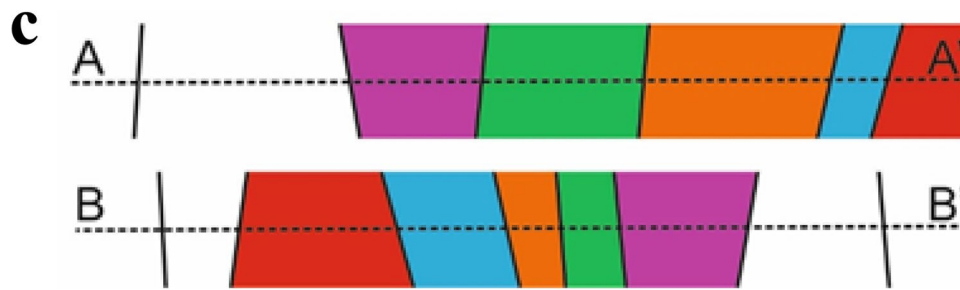


Fig. 1 (continued)

measured by probe no. 4 (30% and over 25%, respectively). The analysis of the 56,326 datasets from the measurements show that radon activity concentrations are comparable at each measurement point (Fig. 2b).

In 2018 probe no. 4 registered significantly lower values of  $^{222}\text{Rn}$  activity concentration during the period of disturbance caused by adaptation works conducted in the main corridor of the underground facility. The commencement of these works and the subsequent long-term opening of entrance and exit holes resulted in significant changes to the air circulation conditions between the interior space and the atmosphere, contributing to the reduction of observed concentration levels (Fig. 2b). These observations were further clarified by Fijałkowska-Lichwa and Przylibski (2021).

The recorded values of  $^{222}\text{Rn}$  activity concentration within the Książ tunnels varied from hundreds to thousands of  $\text{Bq}/\text{m}^3$  (Fig. 2a). The results indicate that the  $^{222}\text{Rn}$  activity concentration (Fig. 2b) is comparable throughout the entire facility, with the only noticeable differences occurring in the immediate vicinity of the fault zone (Fig. 2b, probe No. 4). Previous studies conducted by Przylibski and co-authors (2020) have suggested that these differences may be attributed to local variations in the concentration of the mother isotope  $^{226}\text{Ra}$  in the rock. It could also be influenced by tectonic pressure changes in the orogen, resulting from tectonic activity involving alternating compression and extension phases, which in turn leads to fluctuations in radon exhalation from the rocks into the air within the underground tunnels. Przylibski and co-authors (2020) confirmed that gas exchange between the lithosphere and the atmosphere within the workings occurs not only through active fault zones but also through the entire (fractured) surface of the rocks comprising the roof, floor, and side walls of the underground workings (Fijałkowska-Lichwa 2020).

### 2.3. Discrete fracture network (DFN) model

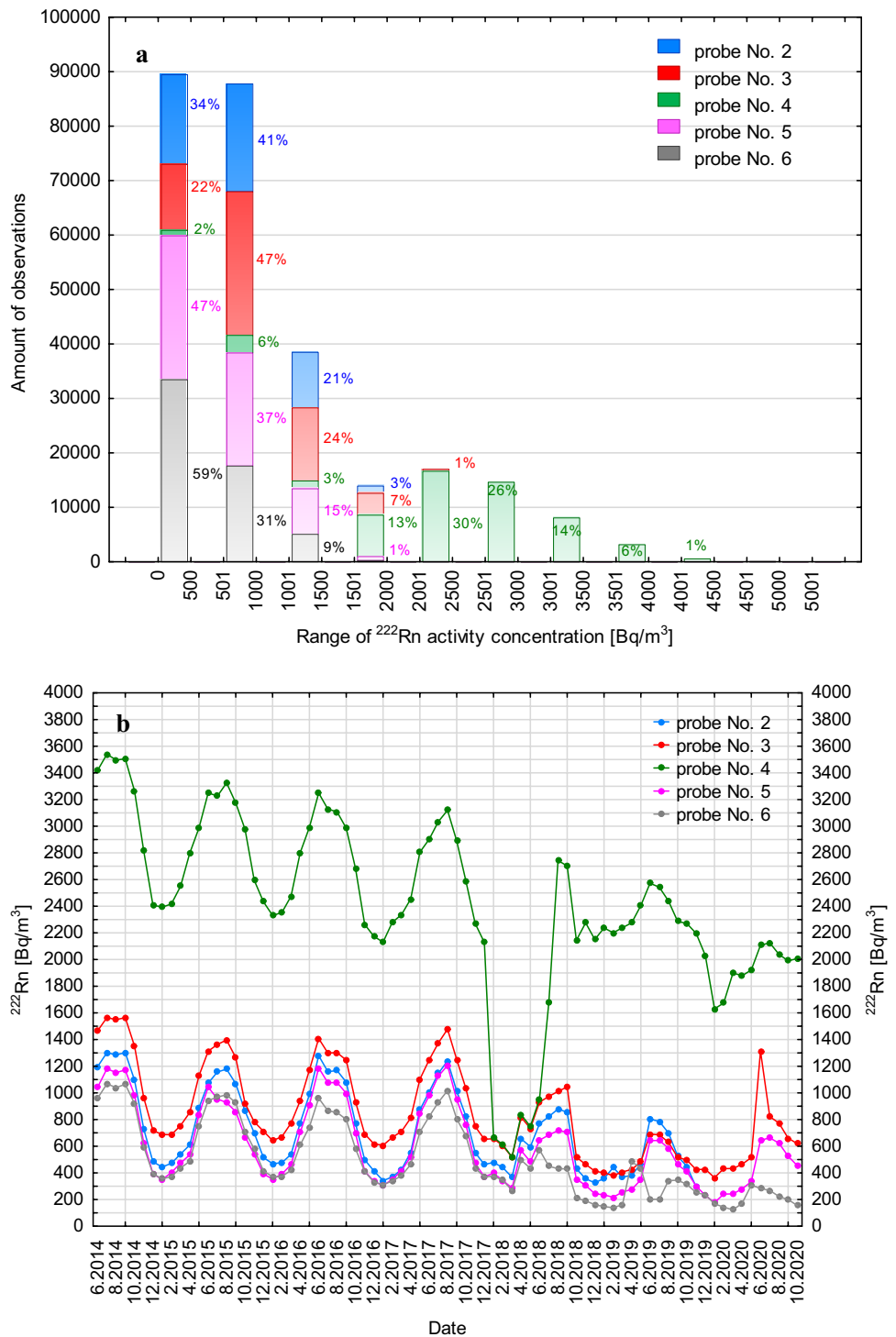
This study utilized the 12 main faults, as described by Kasza and co-authors (2014, 2018), which are visible in two parts of the study site (Fig. 2A), to develop a stochastic Discrete

Fracture Network (DFN) model. Geodetic techniques were employed to measure the dislocation zones. An oriented total station with stabilized points of the horizontal control network was utilized for fault measurements. Kasza and co-authors (2018) identified that most dislocations were accompanied by zones exhibiting intense cataclasis, secondary silification, as well as Fe and Mn mineralization. They further confirmed that the faults were formed due to the reactivation of joint fractures intersecting the steeply dipping (at  $75^\circ$ - $90^\circ$ ) deposits of the Książ Conglomerate Formation (Kasza et al. 2018).

Directional parameters, such as dip and azimuth, were determined and measured for several dozen visible faults within the excavation area of the Książ Massif by Kasza and co-authors (2018). These parameters, combined with archival data from clinometers installed in the Geodynamic Laboratory (GL) of the Space Research Centre of the Polish Academy of Sciences (SRC PAS), allowed for the interpretation and identification of the main fault structures. Consequently, the “creation” of 12 main fault zones was achieved (Fig. 3), following the approach presented by Porębski (1981). According to Porębski, the thickness of the Książ Formation at the study site is estimated to be no less than 2,000 m, which is also supported by the works by Teisseyre (1956, 1968). However, there is a lack of recent field work (boreholes, geophysical research) available from The Polish Geological Institute (PGI) website ([www.pgi.gov.pl/en](http://www.pgi.gov.pl/en)) up until June 2023, which could provide confirmation of this information. Therefore, the simulations and modeling were conducted using a “safe value” of 100 m (depth) and 200 m (width) for the thickness of the Książ Formation. These assumptions align with the morphology of the region of interest, as supported by previous studies and are consistent with the geodetic measurements conducted by Kasza and co-authors (2014, 2018).

Within the modelling area, there are 12 main known faults distributed across different domains, which are incorporated into the model as predefined parameters (Fig. 3). Additional fractures are generated using a stochastic approach, a common method in Discrete Fracture Network (DFN) modelling. The location of fracture centres is modelled using a uniform

**Fig. 2** Distribution of  $^{222}\text{Rn}$  activity concentration at all measurement points (a) along with the course of its variability throughout the measurement period from June 2014 to October 2020 (b). Explanations: points – represent average value of  $^{222}\text{Rn}$  activity concentration, waveform by least squares smoothing

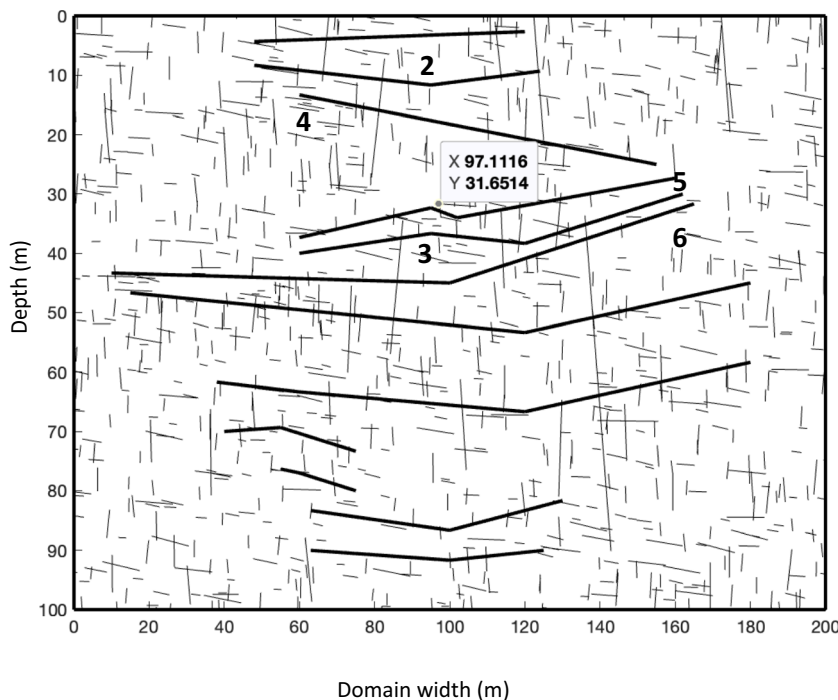


distribution, while the length of fractures follows a power law distribution. The orientation of fractures is modelled using Von-Mises Fisher’s distribution, with a two-set fracture network featuring orientations of 0° and 90°, and a maximum variance of 30°. The stochastic fracture network is generated based on the findings reported by Kasza and co-authors (2018). Figure 3 presents a sample of the DFN model developed with

the stochastically generated fracture network, incorporating the 12 known faults present at the study site. The fracture density is calculated by summing the lengths of fractures and dividing it by the surface area. To estimate the Fracture

and Fault Density (FFD), the area covered by the theoretical 12 main dislocations is assumed to be approximately 150 m x 250 m (equivalent to 37,500 m<sup>2</sup> or 0.0375 km<sup>2</sup>), and the total

**Fig. 3** Discrete fracture network model for the study site with known faults and stochastic fracture network. Fracture network based on Kasza et al. (2018) and Przylibski et al. (2020). Explanations: the numbers 2–6 represent no. of SRDN-3 probe



length of these 12 faults within the modelling area is approximately 1,250 m. Considering that all faults and cracks would be about 3–4 times longer (as suggested by the FFD calculation), the estimated fault length would be around 3–4 times longer than the measured length. For the modelling area, a fracture density of 0.13 m/m<sup>2</sup> is assumed, calculated as 1,250 m (4 times longer) divided by 37,500 m<sup>2</sup>. A fracture density of 0.20 m/m<sup>2</sup> is used to account for potential dead ends in the fracture network that are not included in the length calculation.

**2.4. Radon transport through a fracture network**

Radon transport through a single fracture is affected by the advection, diffusion, radon gas generation and decay as presented in Eq. 1:

$$\frac{\partial c}{\partial t} = \nabla \cdot (D \nabla c) - \nabla \cdot (\vec{V} c) - \lambda c + q \tag{1}$$

In Eq. 1,  $D$  is radon’s coefficient of molecular diffusion (m<sup>2</sup>/s),  $c$  is radon concentration (Bq/m<sup>3</sup>), and  $u$  is advection velocity (m/s),  $\lambda$  is the decay constant(1/s),  $t$  is time in seconds (s),  $V$  is fluid velocity, and  $q$  is radon generation rate (Bq/m<sup>3</sup>s). Assuming a steady, incompressible, and one-dimensional transport of radon along the fracture axis ( $z$ ), Eq. 2 is obtained as:

$$D \frac{\partial^2 c}{\partial z^2} - u \frac{\partial c}{\partial z} - \lambda c + q = 0 \tag{2}$$

Using boundary conditions of  $c(0) = c_o$  and  $c(L) = c_L$ , Ajayi and co-authors (2018) solved for radon flux along a single fracture of length ( $L$ ) and is the sum of flux due to advection and diffusion and it is derived by Fetter and Fetter (1999):

$$J(L) = c_L \delta + c_o \beta - q \phi \tag{3}$$

$$\delta = \frac{1}{2} \left( u - \sqrt{u^2 + 4\lambda D} \coth(\gamma) \right), \beta = \frac{e^{\frac{uL}{2D}}}{2} \left( \sqrt{u^2 + 4\lambda D} \operatorname{csch}(\gamma) \right), \phi = \frac{(\delta + \beta - u)}{\lambda}, \gamma = \sqrt{\left( \frac{uL}{2D} \right)^2 + \frac{\lambda L^2}{D}}$$

Equation 3 describes the radon flux along an individual fracture; however, fractures are often interconnected through a network. Figure 4 presents a simplified representation of a fracture network consisting of two internal nodes (1–7) and three external nodes (8–15). In this network, the radon

activity concentration at the external nodes is assumed to be known and assigned default values. However, the concentrations at the internal nodes remain unknown, and a mass balance approach is applied at these internal nodes to predict the radon activity concentrations:

$$\sum_{i=1}^n J_{i-j} = 0 \tag{4}$$

For the simple discrete fracture network in Fig. 4, Eq. 5 is obtained by applying mass balance at the internal nodes:

$$\begin{bmatrix} \delta_{8-1} + \delta_{9-1} + \delta_{2-1} & \beta_{2-1} & 0 & 0 & 0 & 0 & 0 & 0 \\ \beta_{1-2} & (\delta_{1-2} + \delta_{15-2} + \delta_{3-2}) & \beta_{3-2} & 0 & 0 & 0 & 0 & 0 \\ 0 & \beta_{2-3} & (\delta_{2-3} + \delta_{4-3} + \delta_{5-3}) & \beta_{4-3} & \beta_{5-3} & 0 & 0 & 0 \\ 0 & 0 & \beta_{3-4} & (\delta_{3-4} + \delta_{7-4} + \delta_{14-4}) & 0 & 0 & \beta_{7-4} & 0 \\ 0 & 0 & 0 & 0 & (\delta_{10-5} + \delta_{6-5}) & \beta_{6-5} & 0 & 0 \\ 0 & 0 & 0 & 0 & \beta_{5-6} & (\delta_{5-6} + \delta_{11-6} + \delta_{7-6}) & \beta_{7-6} & 0 \\ 0 & 0 & 0 & \beta_{4-7} & 0 & \beta_{6-7} & (\delta_{6-7} + \delta_{4-7} + \delta_{13-7}) & c_7 \end{bmatrix} \begin{bmatrix} c_1 \\ c_2 \\ c_3 \\ c_4 \\ c_5 \\ c_6 \\ c_7 \end{bmatrix} = \begin{bmatrix} q\phi_{8-1} + q\phi_{9-1} + q\phi_{2-1} - c_8\beta_{8-1} - c_9\beta_{9-1} \\ q\phi_{1-2} + q\phi_{3-2} + q\phi_{15-2} - c_{15}\beta_{15-2} \\ q\phi_{2-3} + q\phi_{4-3} + q\phi_{5-3} \\ q\phi_{3-4} + q\phi_{7-4} + q\phi_{14-4} - c_{14}\beta_{14-4} \\ q\phi_{10-5} + q\phi_{6-5} - c_{10}\beta_{10-5} \\ q\phi_{5-6} + q\phi_{11-6} + q\phi_{7-6} - c_{11}\beta_{11-6} \\ q\phi_{6-7} + q\phi_{13-7} + q\phi_{4-7} + q\phi_{12-7} - c_{13}\beta_{13-7} - c_{12}\beta_{12-7} \end{bmatrix} \tag{5}$$

The advection velocity ( $u$ ) in Eq. 2 is a crucial parameter that can be determined through the application of the cubic law, utilizing uniform values from the literature, or utilizing the Peclet number ( $Pe$ ). To simplify the modeling process, a uniform advection velocity can be assumed, and corresponding values from the literature can be assigned. However, this approach has limitations, particularly when considering the presence of known faults at the study site, as these faults may exhibit different velocity characteristics compared to other fractures within the rock formation. The use of the cubic law can alleviate this limitation; however, it may introduce a bias in the velocity distribution, favoring regions where a higher-pressure head is applied to establish a pressure gradient. Another viable alternative is the utilization of the Peclet number ( $Pe$ ), which is a dimensionless parameter employed to compare the mass transport achieved through advection to that achieved through dispersion or diffusion (Wels et al. 2003). The Peclet number is defined as follows:

$$(Pe) = \frac{uL}{D} \tag{6}$$

The advection velocity for each fracture in the network is calculated by assigning a Peclet number to the model, using Eq. 6. As a case study, Fig. 5a, and 5b illustrate the distribution of advection velocity for a fracture network generated with Peclet numbers of 0.1 and 1, respectively. In Fig. 5a, for a Peclet number of 0.1, the velocities range from  $10^{-8}$  m/s to  $10^{-6}$  m/s.

Similarly, Fig. 5b shows a velocity range of  $10^{-7}$  m/s to  $10^{-4}$  m/s. This aligns with expectations, as a Peclet number of 1 implies higher advection velocities compared to a Peclet number of 0.1. In general, a Peclet number of 1 indicates that

the impact of advection and diffusion are the same. These advection velocities are compared with field measurements conducted at different locations. For example, airflow studies at a rock pile from a former uranium mine at Nordhalde reported a velocity of  $2.3148 \times 10^{-6}$  m/s (Benoit et al. 1991). Advection velocities presented in the literature for various sites (McPherson 1993; Chakraverty et al. 2018; Feng et al. 2021; S3oki et al. 2022) range from  $3.5 \times 10^{-8}$  m/s to  $4.64 \times 10^{-7}$  m/s. Based on these comparisons, a Peclet number of 0.1 is selected for this study. In Eq. 3,  $q$  represents the radon generation rate ( $Bq/m^3s$ ) and represents the radon flux along the fractures per unit aperture. Several factors, such as

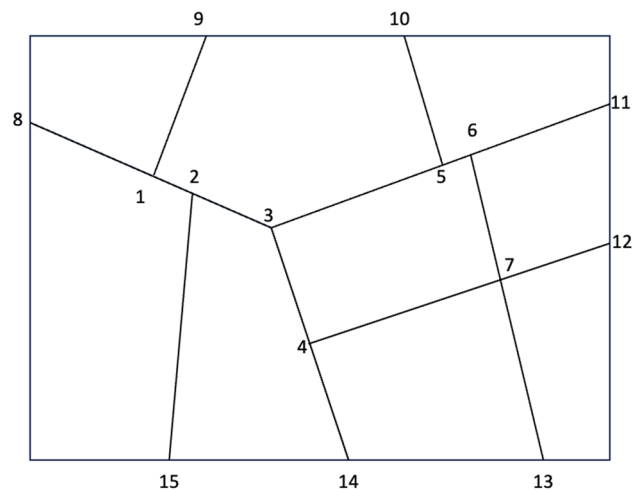
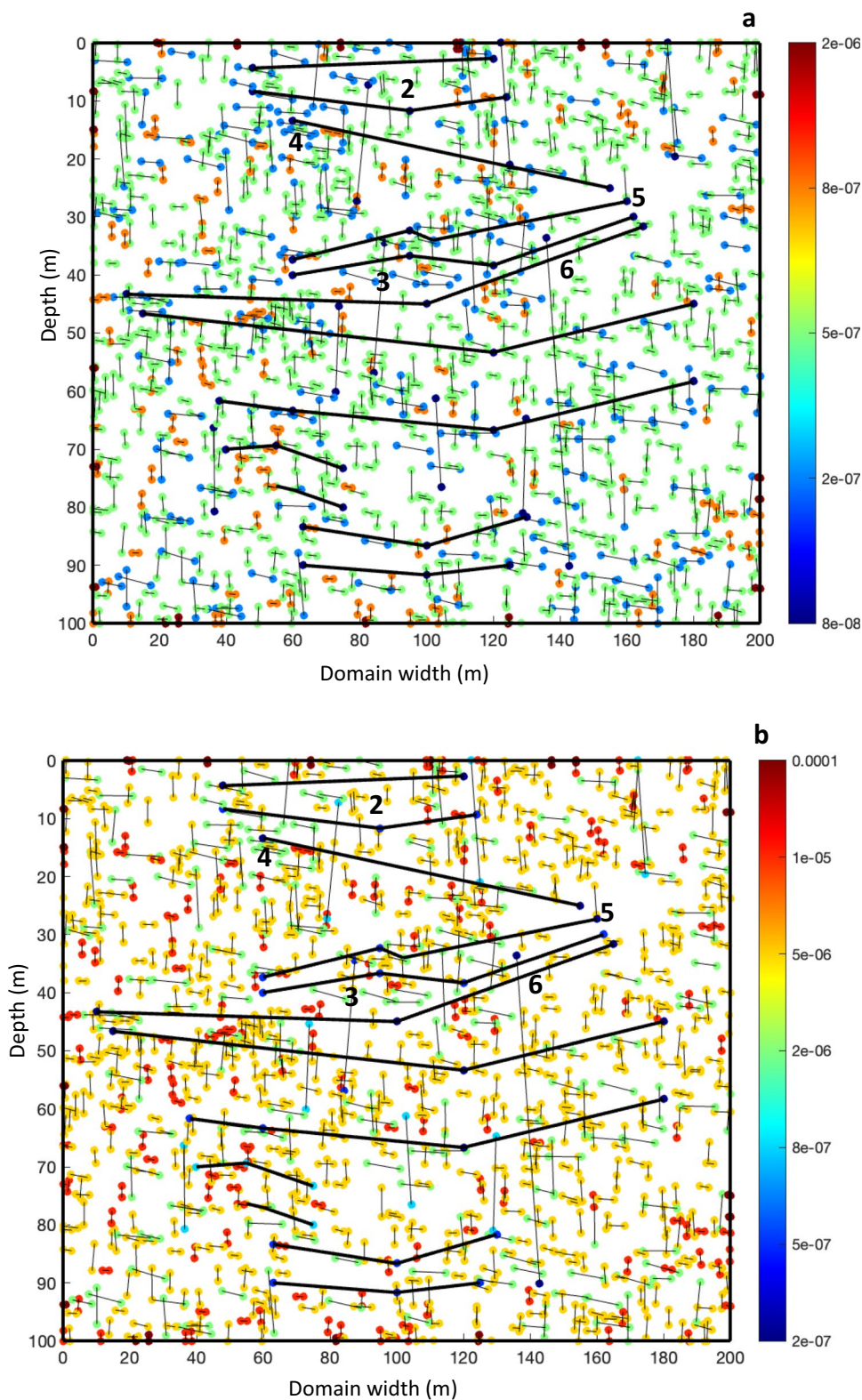


Fig. 4 Conceptualized simple DFN model used to illustrate gas transport. Explanations: 1–7 – internal nodes and 8–15 external nodes

**Fig. 5** Velocity distribution through the fracture network using [a]  $Pe=0.1$ , [b]  $Pe=1$ . Explanations: the numbers 2–6 represent no. of SRDN-3 probe. Fracture network based on Kasza et al. (2018) and Przylibski et al. (2020)



particle soil grain size (Yang 2021), water content (Cozmuta et al. 2003; Yang et al. 2021), porosity (Kumar and Chauhan 2017; Linares-Alemparte et al. 2019), the internal structure of the soil, mineralization type, porosity and permeability

of the soil, and emanation coefficient (Ayman and Tayseer 2019; Azeez et al. 2021), can impact the radon exhalation rate of porous media. For this study, a value ranging from  $1.5 \times 10^{-3}$  to  $3.5 \times 10^{-3}$  Bq/m<sup>3</sup>s is assigned along the fracture

network. Additionally, a 40% higher value is assigned to the region surrounding the fourth probe, where consistently higher radon concentrations have been measured.

## 2.5. Model assumptions and boundary conditions

The fracture network within a rock mass is typically more intricate than depicted in Fig. 4, making it challenging to precisely represent in a model. The challenge lies in the impracticality of fully representing all fractures within a rock mass due to various unknown factors such as fracture length, density, aperture, location, and orientation. Moreover, the connectivity of fractures, influenced by factors like the number of fracture sets, in-situ and induced stress, and fracture density, adds another layer of complexity. Additionally, uncertainties regarding fluid transport parameters, such as the presence of water or other gases, further complicate the modeling process. To address these complexities, Discrete Fracture Network (DFN) models often incorporate stochastic elements and consider known site conditions, including faults. This stochastic approach entails using verified distributions to represent fracture parameters. Typically, fracture length is modeled using a power law distribution, fracture orientation with a von Mises–Fisher distribution, and the location of fracture centers with a uniform distribution.

At this study site, radon measurements have been carried out in both the immediate proximity of a significant fault zone and various smaller, sporadic deformations within the entire excavation system (Fijałkowska-Lichwa and Przylibski 2016; Przylibski et al. 2020). Therefore, a deterministic and stochastic approach was used to develop the DFN model with the incorporation of known faults. The radon diffusion coefficient ( $D$ ) is modeled as  $1.1 \times 10^{-5} \text{ m}^2/\text{s}$  (McPherson 1993) through the fractures like the condition in air. The diffusion coefficient of radon can vary depending on the medium, particularly if the rock unit is saturated with a different fluid. In this study, the transport behavior of fractured rock is simulated under the assumption that it behaves similarly to air, disregarding the presence of other fluids. The presence of water or any other fluid within the rock can significantly affect the diffusion coefficient utilized in this modeling. Nevertheless, according to field measurements conducted near the prominent faults, there is no notable presence of water that could alter the transport properties, despite the possibility of some being trapped within the rock. The radon decay coefficient is modeled as  $2.1 \times 10^{-61}/\text{s}$ . Kasza and co-authors (2018) have noted that the identified faults are filled with clay gouge, occasionally calcified, and contain impregnations of hematite mineralization. To consider these characteristics, the hydraulic aperture is employed, which is typically a fraction of the fracture's maximum opening, known as the mechanical aperture. The mechanisms of gas migration in homogeneous medium include diffusion and advection. But in the faults and in porous media

model of radon migration include gas permeability of soils related to the total porosity, water saturation, and arithmetic fraction (since 1980s). Most of the fluid flow in fractured rock tends to be carried by a tiny of the all fractures (Chen et al. 2023). Based on to the difference in water content, the fractures are divided roughly into two categories: unsaturated and saturated. We assumed that are fractures zones are unsaturated and could be saturated in different depths. So, the mechanisms of gas transport in such different conditions could be determined by diffusion and advection, and also the conventional model. In saturated zones the radon flow is connected with groundwater flows through a fracture-rich rock, gases dissolving in the water released as bubbles with the fracture opening, pressure, or temperature conditions changing (multiphase flow). In unsaturated fractured zones, convection influences radon migration in addition to diffusion. This phenomenon was very widely described by Miklayev et al. (2022). They observed that radon variations in air close correlated with changes in air temperature, and to a lesser with changes in soil moisture. Radon concentration in groundwater varied throughout the year in a relatively narrow range without clear seasonal variations. This confirmed that seasonal variations of soil radon exhalation at the fault zone are not related to the groundwater gas transport. The results of studies indicated that the most likely cause of seasonal variations in the radon values at the fault zone is the inversion of the direction of the convective air flows. The authors observed the convective air flow is directed from fractures and fissures in summer period. The release of radon-carrying air may form abnormal radon levels in soil gas and the surrounding atmosphere. But in winter, on the contrary, atmospheric air is sucked into the fractures of the mountain massif, resulting in a significant decrease in the soil gas radon concentration and suppression of radon exhalation from surface. Radon monitoring conducted over 4-years in research site showed, in our opinion, similarity in the nature of radon activity concentration changes. Therefore, the assumption in the is consistent with the proposal of Miklayev and co-authors (2022).

The main source of radon is strongly fractured Upper-Devonian and Lower-Carboniferous gneiss conglomerates (Przylibski 2005; Wołkowicz 2007). Based on correlation analyses made by Al-Shboul (2023), the amount of Ra-226 in soil significantly influences the radon exhalation rate. Al-Shboul (2023) confirmed that higher moisture levels and greater fine particles in the soil are associated with lower radon exhalation rates. Al-Shboul (2023) stated that the water presence modifies the air volume in the soil and the tortuosity of the pore system, thereby influencing radon diffusion and possibly making it more difficult for radon atoms to reach the surface. He observed that the gravel particles with larger pore spaces associate with higher radon exhalation rates. Therefore, in our perspective, gneiss conglomerates rich in radium-226 suggest obtaining similar results. In this study, the transport behavior of fractured rock is simulated under

the assumption that it behaves similarly to air (Miklayev et al. (2022), disregarding the presence of other fluids.

### 3. Results and discussion

This section presents the findings derived from the developed methodology in this study for predicting <sup>222</sup>Rn activity concentration at the study site, where main faults, fault

zones, and numerous smaller cracks are present in all excavations. The calibration process is extensive, involving adjustment of several parameters to achieve comparable results. However, this study ensures that all parameters fall within a range clearly identified in the literature. The model utilizes the advection velocity distribution described in Fig. 5b, as explained in Section 2.4. A critical parameter for model calibration is the radon generation rate (*q* in Eq. 1), which is extensively discussed in Section 2.4. These two

**Fig. 6** Radon activity concentrations through the rock mass for  $q = 2.4 \times 10^{-3} \text{ Bq/m}^3\text{s}$ . The range of color bar is for clear distinction: values lower than or equal to  $400 \text{ Bq/m}^3$  are dark blue and values greater than or equal to  $1600 \text{ Bq/m}^3$  are dark red. Fracture network based on Kasza et al. (2018) and Przylibski et al. (2020)

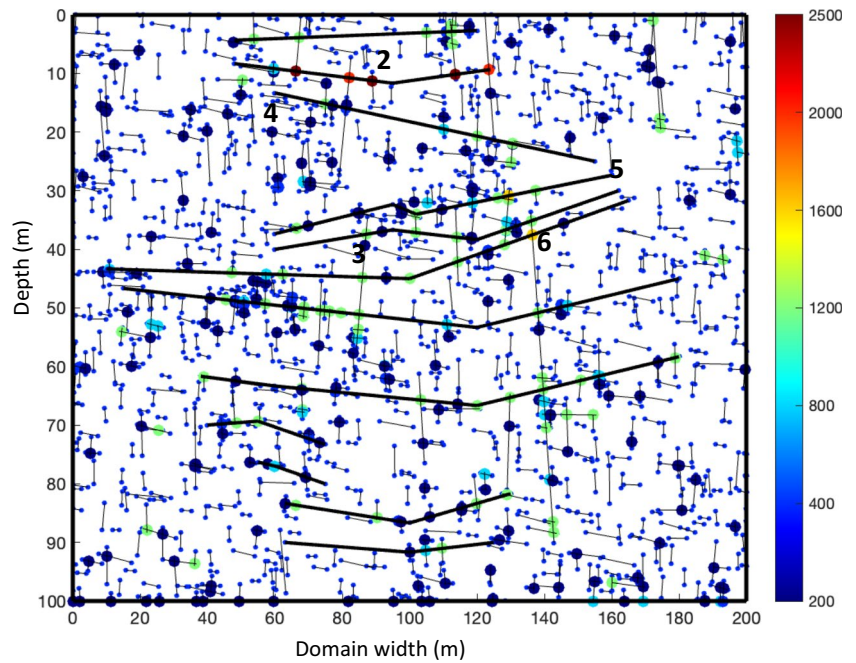


**Fig. 7** Radon activity concentrations through the rock mass for  $q = 3.0 \times 10^{-3} \text{ Bq/m}^3\text{s}$ . The range of color bar is for clear distinction: values lower than or equal to  $400 \text{ Bq/m}^3$  are dark blue and values greater than or equal to  $2000 \text{ Bq/m}^3$  are dark red. Fracture network based on Kasza et al. (2018) and Przylibski et al. (2020)

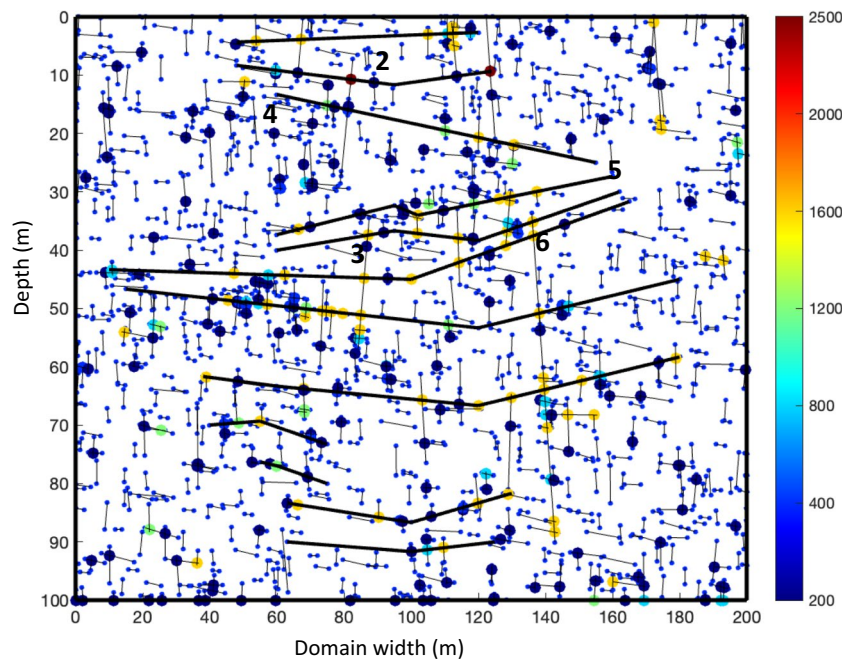
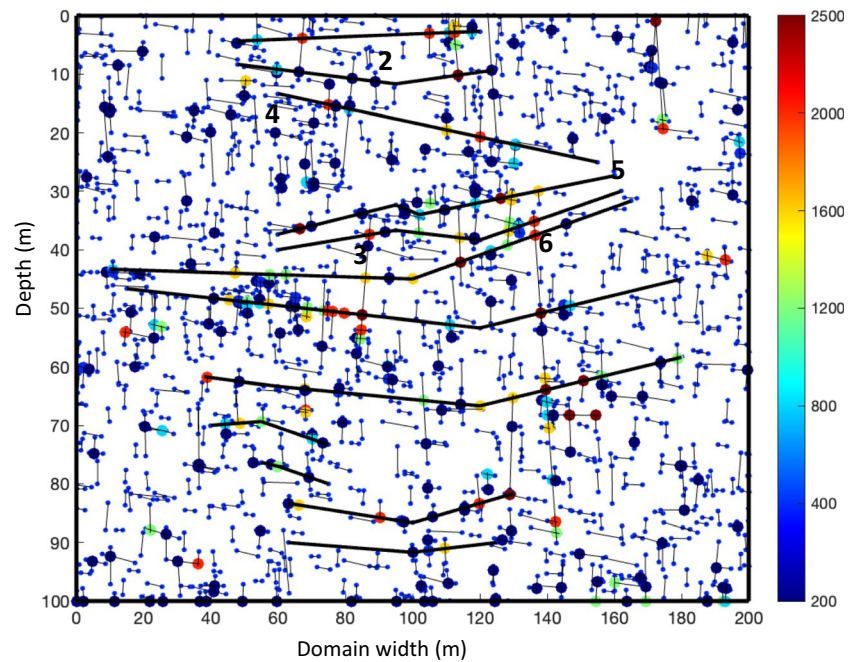


**Fig. 8** Radon activity concentrations through the rock mass for  $q = 1.5 \times 10^{-3} \text{ Bq/m}^3\text{s} - 3.5 \times 10^{-3} \text{ Bq/m}^3\text{s}$ . The range of color bar is for clear distinction: values lower than or equal to  $400 \text{ Bq/m}^3$  are dark blue and values greater than or equal to  $2000 \text{ Bq/m}^3$  are dark red. Fracture network based on Kasza et al. (2018) and Przylibski et al. (2020)



parameters play a significant role in model calibration and can vary considerably across different sites. To initialize the model, a constant radon generation rate ( $q = 2.4 \times 10^{-3} \text{ Bq/m}^3\text{s}$ ) is applied uniformly throughout the rock mass, allowing for observation of variations in  $^{222}\text{Rn}$  activity concentration values with changes in the advection velocity model depicted in Fig. 5b. Figure 6 illustrates the radon concentration map obtained from the numerical model developed for the study site, along with the probe locations, using a radon generation rate of  $q = 2.4 \times 10^{-3} \text{ Bq/m}^3\text{s}$ . Similarly, Fig. 7 presents a concentration map using a higher constant radon generation rate ( $q = 3.0 \times 10^{-3} \text{ Bq/m}^3\text{s}$ ), while Fig. 8 demonstrates the implementation of varied radon generation rates ( $q$ ) ranging from  $q = 1.5 \times 10^{-3} \text{ Bq/m}^3\text{s}$  to  $3.5 \times 10^{-3} \text{ Bq/m}^3\text{s}$ . The model showcases an average distribution of radon gas concentration initialized at  $200 \text{ Bq/m}^3$ .

The results show radon activity concentration at steady state. Although this condition could be transient, field observations indicate that radon fluctuation within a day is not significant. In Fig. 6, the steady-state concentration reveals higher levels of radon activity near faults and particularly in the vicinity of probe 4, as observed in the field. To assess the model's sensitivity to changes in radon generation rate throughout the rock mass, Fig. 7 displays the steady-state outcome for a higher and constant radon gas generation rate. The results in Fig. 7 exhibit higher radon concentrations compared to Fig. 6. This finding supports and validates the previous observation that variations in radon concentrations may be linked to the generation rate within the rock mass. As radon's parent source is uranium, its distribution across the rock mass is non-uniform. This further explains why certain locations may experience elevated radon activity

concentrations. Furthermore, the results emphasize the importance of calibrating the model to align with field measurements, demonstrating that the observations fall within the range of over 50,000 radon activity concentration measurements obtained from field measurements. As mentioned in Section 2.4, a 40% higher radon gas generation rate ( $q$ ) is applied to the area surrounding the fourth probe. Consequently, the results indicate elevated levels of radon concentration near the fourth probe, as depicted in Figs. 6, 7 and 8.

Based on measurements between late spring and autumn (from May to October),  $^{222}\text{Rn}$  activity concentration values ranged from  $800 \text{ Bq/m}^3$  to  $1200 \text{ Bq/m}^3$ , and even  $3200 \text{ Bq/m}^3$  in the vicinity of the main fault (probe No. 4). Between November and April, values of  $^{222}\text{Rn}$  activity concentration are lower, ranging from  $500 \text{ Bq/m}^3$  to  $1000 \text{ Bq/m}^3$  and  $2700 \text{ Bq/m}^3$  next to the main fault (probe No. 4). It shows that the  $^{222}\text{Rn}$  activity concentrations values vary at each measurement site. It found out that the comparable values are measured in the entire excavation system, correspondingly higher in the warmer period and lower in the colder period of the year (Fig. 2b). Comparing these values to measurement results registered by probe no. 4 (located directly at the fault), it was noticed that they are almost 50% higher than for probes no. 2, 3, 5, and 6. From May to October the average radon activity concentration values ranged from  $600 \text{ Bq/m}^3$  to over  $1000 \text{ Bq/m}^3$  (probes no. 2, 3, 5 and 6). The values measured in this time by probe no. 4 is over  $2500 \text{ Bq/m}^3$ . Based on 25,862 data recorded between April and November, the average radon activity concentration values are in the range  $340\text{--}620 \text{ Bq/m}^3$ . But for probe no. 4, the average concentration value is over  $2000 \text{ Bq/m}^3$ . It has been observed that the significant variation in the radon activity concentration values occurred

in 2 periods during a year: November–April (lower), May–October (higher), but not all measuring devices registered the same range of values. Because the observed values of  $^{222}\text{Rn}$  activity concentration varies, the radon gas generation rates cannot be assumed as constant in the main fault vicinity. All these conditions could be studied independently using the developed model. Radon generation rate should be higher for the area where the highest radon activity concentrations were measured. In addition, its value should be higher from 18.5 to 40% between November and April, and from 25 to 37.5% between May and October compared to places where probes (no. 2, 3, 5, and 6) registered significantly lower radon activity concentration values.

In Fig. 8, a simulation is presented with a random distribution of radon generation rates ranging from.

$1.5 \times 10^{-3} \text{ Bq/m}^3 \cdot \text{s}$  to  $3.0 \times 10^{-3} \text{ Bq/m}^3 \cdot \text{s}$  across the rock mass. It was discovered that this calibration leads to a more realistic distribution of  $^{222}\text{Rn}$  activity concentration, resembling the field measurements. The concentration distribution depicted in Fig. 8 reflects a more realistic scenario where the radon generation rate varies throughout the rock mass. This approach allows for a more dispersed concentration pattern, where both the advection velocity and radon generation rate can influence the radon flux. It is recommended that future studies adopt a similar approach, as demonstrated in Fig. 8, to ensure a better representation of field conditions.

The obtained results showed variations of radon exhalation rate with depth of rock mass. With the depth increased, the radon activity concentration value followed by a decreasing trend. Radium-226 present in the stratum rich of gneiss conglomerates is released by a large number of fissures which are used as transport channels for the transfer of free radon gas inside the stratum and finally to the underground atmosphere, forming atmosphere of a highly radon activity concentration. It seems that radon migration takes place as: radon in pore air (mainly) and also in deeper parts as radon dissolved in pore water. The free migration of radon gas occurs in the internal pores and fissures of each stratum in whole rock mass. As the degree of compression increased, the pore air in internal fissures acts as the major medium of propagation for radon, and free radon attached to it starts moving quickly. The opposite situation may occur during rock mass tension. At the same time, the mutual migration of free radon gas also occurs between the different lithologies (cracked and solid mass) and the radon gas in the deep stratum migrated to the shallow stratum and was finally released into the underground atmosphere. It can be assumed that the migration of free radon gas outside the fault's matrix occurs by diffusion through the small pores, cracks, fissures inside each stratum of rock mass. The number of dislocations (deformation) and macroporosity degree of gneiss conglomerates should be recognize as the major storage spaces for free radon. It seems to be confirmed by obtained

seasonal fluctuations of radon activity concentration and radon exhalation rate. The changes are caused by inversion of the convective radon flow directed from the interior of the underground object to atmosphere in winter, and from the atmosphere to underground object inside in summer. The anomalies resulted from the temperature difference between the facility air and atmospheric air.

## 4. Conclusions

This study introduces a developed Discrete Fracture Network (DFN) model aimed at predicting radon concentrations in a study site in Poland. The model utilizes field radon concentration measurements conducted over the past four years, incorporating known faults, and generating additional fracture networks using a stochastic approach. The velocity distribution used in the model is established based on a diffusion dominant transport mechanism, indicated by a Peclet number of 0.1. Calibration of the model basis on over 50,000 radon data includes adjusting the radon generation rate within the range of  $1.5 \times 10^{-3} \text{ Bq/m}^3 \cdot \text{s}$  to  $3.5 \times 10^{-3} \text{ Bq/m}^3 \cdot \text{s}$ .

Calibration of the DFN model made it possible to determine the radon generation rate in the excavation system. The rock mass breathes in its entirety, with a variable radon generation rate. It has been confirmed that the radon generation rate value should be increased up to 40% in places with elevated radon activity concentration values compared to other parts of the facility, where the recorded values are significantly lower both in the warmer (May–October) and colder (November–April) periods of the year. Furthermore, the modeling results indicated that the influence of fracture zones on the recorded concentrations was noticeable up to a depth of 15 m. Within this range, the highest values of  $^{222}\text{Rn}$  activity concentration, ranging from  $1600 \text{ Bq/m}^3$  to  $2000 \text{ Bq/m}^3$ , were consistently observed regardless of the season. However, as the depth increased, the values of  $^{222}\text{Rn}$  activity concentration decreased from  $800 \text{ Bq/m}^3$  to  $400 \text{ Bq/m}^3$  and became more dispersed.

The method developed is implemented in code developed for this study. The results demonstrate that the model shows radon concentration values within a similar range to the field measurements. This successful validation indicates that the method and model developed could have further application in the investigations of different transport parameters on radon flux. Potential future studies using this model could explore seasonal variations in radon concentrations, the influence of fracture water saturation on radon flux, and the effects of diffusion/advection using the Peclet number. Overall, this study presents a realistic and simplified numerical approach for predicting radon concentrations, providing an alternative to resource-intensive field work, and offering expanded investigative potential. However, it is important to note that for application to different study sites, an appropriate calibration specific to each site is necessary.

**Acknowledgements** The authors extend special thanks to researchers who are involved in research in Książ's undergrounds: Prof. Tadeusz A. Przylibski, and PhD Damian Kasza representing the Wrocław University of Science and Technology. The authors extend special thanks to Prof. Marek Kaczorowski from the Geodynamic Laboratory (GL) of the Space Research Centre of the Polish Academy of Sciences (SRC PAS) in Warsaw.

**Author contributions** The authors contributed to the study conception and design. Material and radon database preparation and radon data analysis were performed by the first author. The Fractal Discrete Fracture Network Model was performed by the second author. The first draft of the manuscript was written by both authors. The first author commented and suggested corrections to the first version of the manuscript. Both authors read and approved the final manuscript. Both authors interpreted the results of statistical analyses.

**Data availability** All relevant data and materials are presented in the paper.

## Declarations

**Ethical approval** Not applicable.

**Conflict of interest** The authors state that there are no conflicts of interest regarding the publication of this article and that there are no financial ties to disclose.

**Informed consent** Consent for publication was obtained.

**Disclaimer** The findings and conclusions in this paper are those of the authors and do not necessarily represent the official position of the National Institute for Occupational Safety and Health, Centers for Disease Control and Prevention. Mention of any company or product does not constitute endorsement by NIOSH.

**Open Access** This article is licensed under a Creative Commons Attribution 4.0 International License, which permits use, sharing, adaptation, distribution and reproduction in any medium or format, as long as you give appropriate credit to the original author(s) and the source, provide a link to the Creative Commons licence, and indicate if changes were made. The images or other third party material in this article are included in the article's Creative Commons licence, unless indicated otherwise in a credit line to the material. If material is not included in the article's Creative Commons licence and your intended use is not permitted by statutory regulation or exceeds the permitted use, you will need to obtain permission directly from the copyright holder. To view a copy of this licence, visit <http://creativecommons.org/licenses/by/4.0/>.

## References

- Ajayi K, Shahbazi K, Tukkaraja P, Katzenstein K (2018) A discrete model for prediction of radon flux from fractured rocks. *J Rock Mech Geotech Eng* 10:5:879–892
- Al-Shboul KF (2023) Unraveling the complex interplay between soil characteristics and radon surface exhalation rates through machine learning models and multivariate analysis. *Environ Pollut* 336:122440
- Alhamdi WA, Abdullah KMS (2021) Determination of Radium and Radon Exhalation Rate as a function of soil depth of Duhok Province – Iraq. *J Radiation Res Appl Sci* 14:1:486–494. <https://doi.org/10.1080/16878507.2021.1999719>
- Alvarez-Gallego M, Garcia-Anton E, Fernandez-Cortes A, Cuezva S, Sanchez-Moral S (2015) High radon levels in subterranean environments: monitoring and technical criteria to ensure human safety (case of Castanar cave, Spain). *J Environ Radioact* 145:19–29
- Ambrosino F, Thinová L, Briestenský M, Sabbarese C (2020) Study of  $^{222}\text{Rn}$  continuous monitoring time series and dose assessment in six European caves. *Radiat Prot Dosimetry* 191–2:233–237
- Ayman MA, Tayseer IA (2019) Estimation of radiologic hazards of radon resulting from ceramic tiles used in Najran city. *J Radiation Res Appl Sci* 12:1:210–218. <https://doi.org/10.1080/16878507.2019.1635759>
- Azeez HH, Mohammed MA, Abdullah GM (2021) Measurement of radon concentrations in rock samples from the Iraqi Kurdistan region using passive and active methods. *Arab J Geosci* 13:5:7. <https://doi.org/10.1007/s12517-021-06937-3>
- Barbosa SM, Zafrir H, Malik U, Piatibratova O (2010) Multiyear to daily radon variability from continuous monitoring at the Amran tunnel, southern Israel. *Geophys J Int* 182:2:829–842. <https://doi.org/10.1111/j.1365-246X.2010.04660.x>
- Benoit JM, Torgersen T, O'Donnell J (1991) An advection/diffusion model for  $^{222}\text{Rn}$  transport in near-shore sediments inhabited by sedentary polychaetes. *Earth Planet Sci Letter* 105:4:463–473
- Chakraverty S, Sahoo BK, Rao TD, Karunakar P, Sapra BK (2018) Modelling uncertainties in the diffusion-advection equation for radon transport in soil using interval arithmetic. *J Environ Radioact*. 182. <https://doi.org/10.1016/j.jenvrad.2017.12.007>
- Chen X, Liu Y, Jiang Y, Feng S (2023) Radon transport carried by geogas: prediction model. *Environ Sci Pollut Res* 30:86656–86675. <https://doi.org/10.1007/s11356-023-28616-4>
- Cozmuta I, Van der Graaf ER, De Meijer RJ (2003) Moisture dependence of radon transport in concrete: measurements and modeling. *Health Phys* 85:4:438–456
- Dehghani R, Fathabadi N, Kardan M, Mohammadi M, Atoof F (2013) Survey of gamma dose and radon exhalation rate from soil surface of high background natural radiation areas in Ramsar, Iran. *J Res Med Sci* 15:9:81–84
- Feng S, Wang H, Cui Y, Ye Y, Liu Y, Li X, Wang H, Yang R (2020) Fractal discrete fracture network model for the analysis of radon migration in fractured media. *Comput Geotech* 128:103810. <https://doi.org/10.1016/j.compgeo.2020.103810>
- Feng S, Wu Y, Liu Y, Li X, Wang X, Chen P (2021) A fractal analysis of radon migration in discrete fracture network model. *Chemosphere* 266. <https://doi.org/10.1016/j.chemosphere.2020.129010>
- Fetter CW, Fetter C (1999) *Mass Transport in Saturated Media, in Contaminant hydrogeology*. Prentice Hall New Jersey
- Fijałkowska-Lichwa L (2020) The assessment of lining structure impact on radon behaviour inside selected underground workings under the cour d'honneur of Książ Castle. *J Radioanal Nucl Chem*. <https://doi.org/10.1007/s10967-020-07391-3>
- Fijałkowska-Lichwa L, Przylibski TA (2011) Short-term  $^{222}\text{Rn}$  activity concentration changes in underground spaces with limited air exchange with the atmosphere. [in:] *Nat Hazards Earth Syst Sci* 11:1179–1188
- Fijałkowska-Lichwa L, Przylibski TA (2016) First radon measurements and occupational exposure assessments in underground geodynamic laboratory the Polish Academy of Sciences Space Research Centre in Książ Castle (SW Poland). *J Environ Radioact* 165:253–269
- Fijałkowska-Lichwa L, Przylibski TA (2021) Assessment of occupational exposure from radon in the newly formed underground tourist route under Książ Castle, Poland. *Radiat Environ Biophys* 60:2:329–345
- Fijałkowska-Lichwa L, Przylibski TA (2023) Radon ( $^{222}\text{Rn}$ ) as a tracer in natural ventilation efficiency assessment in underground workings – an example of St John Mine tourist complex

- in Krobica (the sudetes, SW Poland). *J Environ Radioact* 265:107225. <https://doi.org/10.1016/j.jenvrad.2023.107225>
- Gillmore GK, Phillips PS, Denman AR (2005) The effects of geology and the impact of seasonal correction factors on indoor radon levels: a case study approach. *J Environ Radioact* 84:469–479
- Girault F, Viveiros F, Silva C, Thapa S, Pacheco JE, Adhikari LB, Bhattarai M, Koirala BP, Agrinier P, France-Lanord Ch, Zanon V, Vande-meulebrouck J, Byrdina S, Perrier F (2022) Radon signature of CO<sub>2</sub> flux constrains the depth of degassing: Furnas volcano (Azores, Portugal) versus Syabru-Bensi (Nepal Himalayas). *Sci Rep* 12:10837
- Groves-Kirkby CJ, Crockett RGM, Denman AR, Phillips PS (2015) A critical analysis of climatic influences on indoor radon concentrations: implications for seasonal correction. *J Environ Radioact* 148:16–26
- Haquin G, Zafrir H, Ilzyer D, Weisbrod N (2021) Monte Carlo modeling of scintillation detectors for continuous underground radon monitoring. *J Environ Radioact* 237:106693
- Kaczorowski M (1999) The results of preliminary tilt measurements by use of the long water-tube clinometer in Książ Geophysical Station. *Artif Satellites* 34:3:193–201
- Kaczorowski M, Wojewoda J (2011) Neotectonic activity interpreted from a long water-tube tiltmeter record at the SRC Geodynamic Laboratory in Książ, Central Sudetes, SW Poland. *Acta Geodynamica et Geomater* 8:3:249–261
- Kaczorowski M, Olszak T, Walo J, Barlik M (2012) Research of absolute gravity variations on Geodynamic Laboratory in Książ in the period 2007–2011. *Artif Satellites* 47:4:169–176
- Kasza D, Kaczorowski M, Zdunek R, Wronowski R (2014) The damages of Książ Castle architecture in relation to routes of recognized tectonic faults and indications of recent tectonic activity of Świebodziце Depression Orogen – Central Sudetes, SW Poland. *Acta Geodynamica et Geomater* 11(3):175:225–234
- Kasza D, Kowalski A, Wojewoda J, Kaczorowski M (2018) Indicators of recent Geodynamic Activity in the Książ Castle area (Świebodziце Unit, Sudetes) in the light of structural analysis and geodetic measurements. [in: Przylibski TA, and Kasza D (Eds.) XVII Conference of Phd Students and Young Scientists, E3S Web of Conferences 29. <https://doi.org/10.1051/E3Sconf/20182900021> [in Polish]
- Kávási N, Somlai J, Szeiler G, Szabó B, Schafer I, Kovács T (2010) Estimation of effective doses to cave dwellers based on radon measurements carried out in seven caves of the Bakony Mountains in Hungary. *Radiat Meas* 45:9: 1068–1071. <https://doi.org/10.1016/j.radmeas.2010.07.017>
- Kleinschmidt R, Watson D, Janik M, Gillmore G (2018) The presence and dosimetry of radon and thoron in a historical, underground metalliferous mine. *J Sustainable Min* 17:3:120–130
- Kumar A, Chauhan RP (2017) Radon diffusion and exhalation from mortar modified with fly ash: waste utilization and benefits in construction. *J Mater Cycles Waste Manage* 19:1:318–325
- Lei B, Zhao L, Girault F, Cai Z, Luo C, Thapa S, She J, Perrier F (2023) Overview and large-scale representative estimate of radon-222 flux data in China. *Environ Adv* 11:100312
- Li P, Sun Q, Geng J, Shi Q, Hu J, Tang S (2022) A study on the differences in radon exhalation of different lithologies at various depths and the factors influencing its distribution in northern Shaanxi, China. *Sci Total Environ* 849:157935
- Li H, Li F, Wang S (2024) Measurement and characteristics of radon flow in an extremely arid region based on a closed-system earth-air model. *J Environ Manage* 356:120675
- Linares-Alemparte P, Andrade C, Baza D (2019) Porosity and electrical resistivity-based empirical calculation of the oxygen diffusion coefficient in concrete. *Constr Build Mater* 198:710–717
- McPherson MJ (1993) Radiation and Radon gas. *Subsurface Vent Environ Eng*, 457–487
- Miklyayev PS, Petrova TB (2021) Study of abnormal seasonal variations in the Radon Exhalation Rate in a Fault Zone. *Geochem Int* 59:4:435–447
- Miklyayev PS, Petrova TB, Marennyy AM, Shchitov DV, Sidiyakin PA, Murzabekov MA, Lopatin MN (2020) High seasonal variations of the radon exhalation from soil surface in the fault zones (Baikal and North Caucasus regions). *J Environ Radioact* 219:106271
- Miklyayev PS, Petrova TB, Shchitov DV, Sidiyakin PA, Murzabekov MA, Marennyy AM, Nefedov NA, Sapozhnikov YA (2021) The results of long-term simultaneous measurements of radon exhalation rate, radon concentrations in soil gas and groundwater in the fault zone. *Appl Radiat Isot* 167:109460. <https://doi.org/10.1016/j.apradiso.2020.109460>
- Miklyayev PS, Petrova TB, Shchitov DV, Sidiyakin PA, Murzabekov MA, Tsebro DN, Marennyy AM, Nefedov NA, Gavriliev SG (2022) Radon transport in permeable geological environments. *Sci Total Environ* 852:158382
- Miklyayev PS, Petrova TB, Maksimovich NG, Krasikov AV, Klimshin AV, Shchitov DV, Sidiyakin PA, Tsebro DN, Meshcheriakova OY (2024) Comparative studies on radon seasonal variations in various underground environments: cases of abandoned beshtaugorskiy uranium mine and Kungur Ice Cave. *J Environ Radioact* 272:107346. <https://doi.org/10.1016/j.jenvrad.2023.107346>
- Muhammad A, Kùlahcı F (2022) Radon transport from soil to air and Monte-Carlo simulation. *J Atmospheric Solar–Terrestrial Phys* 227:105803
- Pawlikowska M (2008) Książ castle – mysteries of the past as a chance to revive tourist attendance. [in:] *Dziedzictwo Kulturowe - Ochrona i adaptacja jako szansa na rozwój. Koło Naukowe Młodych Geografów „Geoholicy, Uniwersytet Łódzki.* [in Polish].
- Pla C, Fernandez-Cortes A, Cuezva S, Galiana-Merino JJ, Cañaveras S, Sanchez-Moral JC, Benavente D (2020) Insights on climate-driven fluctuations of cave <sup>222</sup>Rn and CO<sub>2</sub> concentrations using statistical and wavelet analyses. *Geofluids* 8858295. <https://doi.org/10.1155/2020/8858295>
- Pla C, Ruiz MC, Gil-Oncina S et al (2023) <sup>222</sup>Rn and CO<sub>2</sub> monitoring in soil and indoor atmosphere to understand changes in the gaseous dynamics of Rull cave (Spain). *Environ Earth Sci* 82:235. <https://doi.org/10.1007/s12665-023-10885-4>
- Porębski SJ (1981) Świebodziце succession (Upper Devonian-Lower Carboniferous. Western sudetes): a prograding mass-flow dominated fan-delta complex. *Geologia Sudet* 16:1:99–190
- Prasetyo R, Hutabarat J, Daud Y, Hendarmawan H (2023) Distribution of <sup>222</sup>Rn and CO<sub>2</sub> across faults and its origin in Wayang Windu geothermal area. West Java – Indonesia *Geothermics* 110:102691
- Przylibski TA (2005) Radon E a specific ingredient of Medicinal Waters. *Oficyna Wydawnicza Politechniki Wrocławskiej, Wrocław.* [in Polish]
- Przylibski TA, Bartak J, Kochowska E, Fijałkowska Lichwa L, Kozak K, Mazur J (2010) New SRDN-3 probes with a semiconductor detector for measuring radon activity concentration in underground spaces. *J Radioanalytical Nuclear Chem* 289:599–609
- Przylibski TA, Kaczorowski M, Fijałkowska-Lichwa L, Kasza D, Zdunek R, Wronowski R (2020) Testing of <sup>222</sup>Rn application for recognizing tectonic events observed on water-tube tiltmeters in underground Geodynamic Laboratory of Space Research Centre at Książ (the sudetes, SW Poland). *Appl Radiat Isot* 163:108967. <https://doi.org/10.1016/j.apradiso.2019.108967>
- Rafique M, Iqbal J, Shah SAA, Alam A, Lone KJ, Barkat A, Shah MA, Qureshi SA, Nikolopoulos D (2022) On fractal dimensions of soil radon gas time series. *J Atmospheric Solar–Terrestrial Phys* 227:105775
- Sajwan RS, Joshi V, Ahamad T, Kumar N, Parmar P, Jindal MK (2024) Assessment of Radon transportation and uranium content in the

- tectonically active zone of Himalaya, India. *Sci Total Environ* 926:171823
- Smetanová I, Barbosa SA, Vďačný M et al (2023) The effect of environmental parameters on radon concentration measured in an underground dead-end gallery (Vyhne, Slovakia). *J Radioanal Nucl Chem* 332:1733–1742. <https://doi.org/10.1007/s10967-023-08884-7>
- Smith ME, Dumitru OA, Burgele BD et al (2019) Radon concentration in three Florida caves: Florida, Jennings, and Ocala. *Carbonates Evaporites* 34:433–439. <https://doi.org/10.1007/s13146-018-0473-7>
- Sóki E, Sándor G, Csige I (2022) Origin and transport of radon in a dry and in a wet mofette of COVASNA, Romania. *J Environ Radioact*. <https://doi.org/10.1016/j.jenvrad.2022.106962>
- Tchorz-Trzeciakiewicz DE, Parkitny T (2015) Radon as a tracer of daily, seasonal and spatial air movements in the underground tourist route coal mine (SW Poland). *J Environ Radioact* 149:90–98
- Teisseyre H (1956) The Świebodzice depression as a geological unit. *Biul Instytutu Geologicznego* 106:1–60 [in Polish]
- Teisseyre H (1968) Stratigraphy and tectonics of the Świebodzice Depression. *Biul Instytutu Geologicznego* 222:77–106 [in Polish]
- Thuamthansanga T, Tiwari RC (2022) Correlation of in-situ online  $^{222}\text{Rn}$  data at Mat fault with geophysical process. *Materials Today: Proceedings*, 65:2825–2831
- Vaupotič J, Gregorič A, Kobač I, Kozak K, Mazur J, Kochowska E, Grządziel D (2010) Radon concentration in soil gas and radon exhalation rate at the Ravne Fault in NW Slovenia. *Nat Hazards Earth Syst Sci* 10:4:895–899. <https://doi.org/10.5194/nhess-10-895-2010>
- Wang H, Xie B, Wang Y, Wen J, Hong C (2024) Influence of temperature on the radon concentration distribution in ramp under low-speed wind field: a numerical simulation study. *J Environ Radioact* 272:107331
- website <https://www.pgi.gov.pl/en/>, accessed March 2023 [in Polish]
- Wels C, Lefebvre R, Robertson AM (2003) An overview of prediction and control of air flow in acid-generating waste rock dumps. in *Proceedings Sixth International Conference on Acid Rock Drainage*. Cairns, QLD, 12–18 July 2003
- Wołkowicz S (ed) (2007) Units of Foreesudetic Block. [in:] *Radon Potential of Sudetes with Determination of Potentially Medicinal Radon Water Areas*. Państwowy Instytut Geologiczny, Warszawa [in Polish]
- Yang R, Zhang X, Feng S, Li X (2021) Influence of neutralization accelerated by the soak method on the radon exhalation of cement-based materials. *Health Phys* 120:2:191–200
- Ye Y, Chen G, Dai X, Huang C, Yang R, Kearfott KJ (2019) Experimental study of the effect of water level and wind speed on radon exhalation of uranium tailings from heap leaching uranium mines. *Environ Sci Pollut Res* 26:25:25702–25711
- Yeamin MB, Islam MM, Chowdhury AN, Awual MR (2021) Efficient encapsulation of toxic dyes from wastewater using several biodegradable natural polymers and their composites. *J Clean Prod* 291:125920
- Żelaźniewicz A, Aleksandrowski P (2008) Tectonic subdivision of Poland: southwestern Poland. *Przegląd Geol* 56:10: 904–911 [in Polish]
- Zheng X, Sun X, Jing X, Yang D, Jia H (2023) Evolution of pore structure and radon exhalation characterization of porous media grouting. *Sci Total Environ* 865:161352. <https://doi.org/10.1016/j.scitotenv.2022.161352>

## Authors and Affiliations

Lidia Fijałkowska–Lichwa<sup>1</sup>  · Kayode M. Ajayi<sup>2</sup> 

✉ Lidia Fijałkowska–Lichwa  
lidia.fijalkowska-lichwa@pwr.edu.pl

Kayode M. Ajayi  
kayodeajayi.m@gmail.com

<sup>1</sup> Faculty of Civil Engineering, Wrocław University of Science and Technology, Wybrzeże S. Wyspiańskiego 27, Wrocław 50–370, Poland

<sup>2</sup> Centers for Disease Control and Prevention, National Institute for Occupational Safety and Health, Pittsburgh, PA 15236, USA